International Journal of Advanced Research in Physical Science (IJARPS)
Volume 7, Issue 6, 2020, PP 3-13
ISSN No. (Online) 2349-7882
www.arcjournals.org

Statistical Evaluation of Global and Ultraviolet Solar Radiation by Using Artificial Neural Networks

U. Ali Rahoma, Samy A. Khalil*, A.H.Hassan, and A. Shaban,

National Research Institute of Astronomy and Geophysics, Helwan, Egypt

Corresponding Author:** ***Samy A. Khalil, *National Research Institute of Astronomy and Geophysics, Hel wan, Egypt*

Abstract: *An attempt was done to describe the ANN outputs in terms of first order polynomials relating clearness index (KT) and sunshine (S). If care is taken in considering the corresponding regional climatic differences, these correlations can be generalized and transferred to other sites. The results hint that the ANN model is more suitable to predict global daily ultraviolet in daily scales than the regression models in the plain areas of Egypt. Intensity variations of global daily ultraviolet (GUVB) radiation throughout the years, 2015-2017 are used. In this study, two different methodologies are used to develop two models for estimating daily solar UVB radiation. The first is based on traditional statistical techniques whereas the second is based on artificial neural network methods. Both models use daily solar global broadband radiation as the only measured input. The statistical model is derived from a relationship between the daily UVB and the global clearness indices but modulated by the relative optical air mass. The inputs to the neural network model were determined from a large number of radiometric and atmospheric parameters using the automatic relevance determination method, although only the daily solar global irradiation, daily global clearness index and relative optical air mass were shown to be the optimal input variables. Results show that the statistical model performs adequately in both sites for all weather conditions, especially when only clear sky days at Golden were considered (RMSE=4.6%, MBE= –0.1%). The neural network-based model provides the best overall estimates in the site where it has been trained, but presents an inadequate performance for the Golden site when snow-covered days are included (RMSE= 6.5%, MBE= –3.0%).*

Keywords: *global solar radiation; atmospheric parameters; UVB solar radiation; neural network; optical air mass; root mean square.*

1. INTRODUCTION

The forecast is extremely valuable in sun oriented vitality applications since it licenses to assess sun oriented information for areas where estimations are not accessible. The created man-made consciousness models anticipate the sun based radiation time arrangement all the more viably contrasted with the customary methods dependent on the clearness file. The estimating capacity of certain models could be additionally improved with the utilization of extra meteorological parameters. In the wake of having recreated a wide range of structures of neural systems and prepared utilizing estimations as preparing information, the best structures were chosen so as to assess their presentation in connection with the exhibition of a neuro-fluffy framework [1-4]. As the elective framework, ANFIS neuro-fluffy framework was considered, on the grounds that it joins fluffy rationale and neural system strategies that are utilized so as to acquire effectiveness. ANFIS is prepared with similar information. The correlation and the assessment of the two frameworks are finished by their forecasts, utilizing a few blunder measurements. Fluffy model was prepared utilizing information of every day sun powered radiation recorded on a level surface in National Research Institute of Astronomy and Geophysics, Helwan, Egypt (NRAIG) at ten years (1991-2000). The anticipating end shows that the TS fluffy model gives a decent exactness of around 96% and a root mean square blunder lower than 6% [5]. The diffuse component considers are essential for most energy applications, can be obtained through various theoretical or empirical correlations. These correlations are usually expressed in terms of linear and/or polynomial fittings relating the diffuse fraction with, (i) the clearness index [6–7] and/or (ii) combining both clearness index and sunshine fraction [8]. One of the limitations imposed by these correlations is that they show a latitude dependency [8-10]. As a result, checked the adequacy of eight widely used linear regression models for the prediction of diffuse fraction in different scales [11]. An integral view of this study shows that:

For the observed range of errors, it was determined that Gopinathan and Soler's model [11] produces the lower error, while Collares-Pereira and Rabl's [10], and Ruth and Chant's [11] models follow in that order. As a result, Gopinathan and Soler's model can be used with confidence to calculate the diffuse fraction in daily scale for Egypt. The analytical form of Gopinathan and Soler's model [11] is given by:

$$k_D = 0.7345 + 0.0219 * k_t - 0.5665 * (\frac{S}{S_0}) \quad (1)$$

The clearness index can be defined on an instantaneous, hourly, or monthly basis, and the values in HOMER's solar resource Inputs window are monthly average values. The symbol for the monthly average clearness index is K_t. In hourly scale it is recommended that the correlations developed by Sokol Dervishi and Ardeshir Mahdavi [12], Marcelo de Carvalho Alves, et al. [13] be used when no recorded data are available. These correlations are given as:

$$k_D = \begin{cases} 1.0 - 0.09 * k_t, & 0 \le k_t \le 0.22, \\ 0.9511 - 0.1604 * k_t + 4.388 * k_t^2 - 16.638 * k_t^3 + 12.336 * k_t^4, & 0.22 < k_t \le 0.8 \\ 0.165, & k_t > 0.8. \end{cases} \quad (2)$$

In opposition to the scientific schedules referenced above fake novel system (ANN) models can help in finding out about the key data designs inside a multi-dimensional data area. Moreover, they are especially reasonable to tackle the issue of distinguishing proof within the sight of boisterous information [14, 15], and some promising results have been reported [16–17]. For those reasons, the problem we address here is to compare the performance of Gopinathan and Soler [10-13] with that of the ANN model, which can be based on K_D and S.

The Ultraviolet sunlight based radiation estimations were done at Cairo and Aswan in Egypt for a long time (1990-1992) utilizing Eppley Ultraviolet Radiometers by the Egyptian Meteorological Authority. Additionally, the worldwide sun oriented radiation was recorded for a similar three years at Cairo and Aswan utilizing Eppley pyranometer. All the meteorological states of the two urban areas were gathered, and the stratospheric ozone was estimated by Dobson spectrophotometers. The proportion of the bright to the worldwide radiation (UV/G) ran between 2.7% in winter to 3.4% in summer for Cairo. Aswan in the south of Egypt shows the opposite where the proportion of bright to worldwide sun based radiation (UV/G) extend between 3.9% in winter to 3.5% in summer (Shaltout et al., 1994 [18]).

2. DATA PREPROCESSING

2.1. Solar Radiation Instruments

Equipment was installed on the roof of NRIAG building in Helwan, (29˚54˜ N 30˚ 20˜ E, 126 m elevation above sea level). The background is taken as desert and pollution. Measurements were conducted from sunrise to sunset. The time of measurements was taken as the local mean time of Cairo (GMT+2 hours). This analysis is based on hourly radiometric data collected at the new building of NRIAG, Helwan, Egypt site, (29°51′31″N 30°15′06″E, 127 m a.m.s.l.) for a 3-year period (2015–2017). Global solar radiation (G, 305–2800 nm) was measured using the Kipp & Zonen model CM11 pyranometer (Delft, The Netherlands). USA), while the ultraviolet solar radiant flux (G_{UVB}, 280–380 nm) readings were obtained by adding Skye's sensors outputs. Daily values for all the radiometric components have been computed by summing the individual radiant fluxes over the course of a day. The daily values of solar radiant fluxes are expressed as: MJ m^{-2} for G, $molm^{-2}$ for PPFD-QP, and kJ m^{-2} for G_{UV}, respectively.

2.2. Weather Station Instruments

The DAVIS weather station (Vantage Pro 2) was installed in October 2010. The Vantage Pro 2 contains two parts: The Integrated Sensor Suite (ISS) that collects outside weather data and Vantage Pro2 console that received wireless data from (ISS). The ISS contains a rain collector, temperature sensor, humidity sensor, anemometer, solar radiation sensor and an ultraviolet (UVB) radiation sensor. The Vantage Pro 2 recorded data every 10 minutes. The next section presents the description and specification of the UVB sensor.

Plan and investigation of fake neural system models dependent on multilayer perceptron for the estimation of day by day sun powered brilliant parts uncover the possibility of this instrument for

anticipating G and G_{UVB} sun based brilliant transitions. Right now just one concealed layer is adequate for evaluating every day worldwide unearthly brilliant motions through both sun based and climatic parameters. Daylight term assumes a significant job in getting satisfactory model forecasts, though different parameters utilized may create clashing impacts on the ANN models' presentation. Looking at measurable outcomes for all ANN-models displayed right now can be reasoned that the models ANN-5 (nN, T, rh) for G_h, ANN-3 (nN, G_h) for QP and ANN-6 (nN, G_h, G_0, O_3, m, T, rh) for G_{UVB} gave the best outcomes. Results got through exactly inferred plans, albeit measurably huge, gave factual exhibitions that are lower contrasted with that gave by the ANN-models occupied with this investigation. At long last, the outcomes acquired right now the ANN procedure as a promising option in contrast to the regular relapse displaying for both broadband and phantom sunlight based brilliant transition expectations.

3. Mathematical Basis of Neural Network Approach

We believe that an understanding of the neural network is essential for the satisfactory and successful use of this model. So we present here a brief review of the ANN model utilized in this study.

3.1. Global solar radiation G

The Angstrom–Prescott model is the most widely used method for G predictions. It is given as,

$$\mathbf{G_h} = \left[\mathbf{a} + \mathbf{b} * \left(\frac{\mathbf{S}}{\mathbf{So}}\right)\right] * \mathbf{G_0} \quad (3)$$

G is the daily average of solar global radiant flux, G_0 is the daily average extraterrestrial radiant flux, S is the measured sunshine hours and S_o is the theoretical sunshine duration for a day, whereas a & b are regression constants. Using daily data for the period 2015–2017 the final form of Eq. (1) for the Cyprus environ is written as:

$$\mathbf{G_h} = \left[\mathbf{0.236} + \mathbf{0.498} * \left(\frac{\mathbf{S}}{\mathbf{So}}\right)\right] * \mathbf{G_0} \quad (4)$$

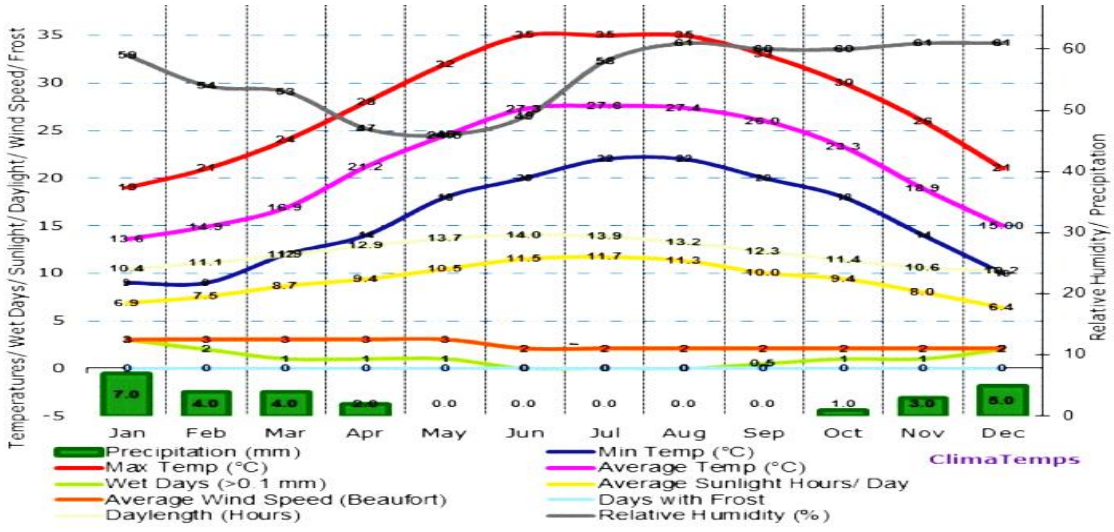

Figure1. *Shows the weather of Cairo has a subtropical desert/low-latitude arid hot climate (BWh) [18].*

Table1. *Annual Variation Ratios of Clearness index, Helwan (2015-2017).*

Month	S	S/S0	K_{TG}	K_{TGUVB}
1.00	7.00	0.68	0.57	0.15
2.00	7.80	0.71	0.63	0.16
3.00	8.40	0.71	0.63	0.22
4.00	9.40	0.74	0.62	0.31
5.00	10.60	0.79	0.63	0.30
6.00	11.80	0.85	0.62	0.33
7.00	11.50	0.84	0.59	0.32
8.00	11.00	0.84	0.60	0.30

9.00	10.10	0.82	0.60	0.29
10.00	9.40	0.83	0.56	0.26
11.00	8.00	0.76	0.57	0.15
12.00	7.00	0.69	0.58	0.12

NRIAG measures and provides solar radiation data along with other climatic parameters over various locations across the country. The data recorded by NRIAG is usually global solar radiation along horizontal axis. Table1. Shows the clearness index data inputs (K_{TG}) of Helwan, sunshine duration, ration of sunshine duration, K_{TGUVB}. The K_{TG} vary between 0.57 - 0.63, K_{TGUVB} vary from 0.12 to 0.33. The spectral composition of the in global solar radiation are: global horizontal UV band (250-385nm) forms 4.3% with standard division (SD) 0.004 and the correlation coefficient CC = 85%. Figure 1 shows the weather of Cairo has a subtropical desert/ low-latitude arid hot climate (BWh) According to classification Cairo is situated in or near the subtropical desert biome. The annual mean temperature is 21.4 degrees Celsius. See the temperatures page for a monthly breakdown and the fixed scale graph. Average monthly temperatures vary by 14 °C. This indicates that the continentally type is oceanic, subtype truly oceanic. Total annual precipitation averages 26 mm (1inches) which is equivalent to 26 Liters/m². On average there are 3451 hours of sunshine per year, as shown in Figure 2.

4. Artificial Neural Network Models

For each solar radiant component, the ANN-models were created. Counterfeit neural systems have been broadly utilized in many research fields. A schematic chart of the fundamental engineering for a run of the mill feed-forward neural system with one concealed layer is shown in Fig. 2. The barometrical parameters are sustained into the model through the info layer and they are sent into the neurons that make up the concealed layer. Each sign that the neuron gets is weighted and the outcomes are first added and afterward sent to the yield layer which is the determined yield of the model. The determined yield is contrasted and the ideal yield and if the mistake is noteworthy, the Levenberg–Marquardt calculation is utilized so as to adjust the loads of the neurons so as to limit the blunder. This system is rehashed until the systems work agreeably or no further improvement is conceivable. As referenced before, the wide point of this investigation is to show and gauge, through utilizing ANN-procedures, the broadband Global sun oriented radiation (G) just as worldwide PAR and UVB phantom brilliant motions, by utilizing of both sun based brilliant and environmental parameters.

Table 2 condenses the ANN-models inferred for the broadband sun powered worldwide G and G_{UVB} sunlight based brilliant parts. Up until now, for the G brilliant motion, the principal model enrolled as ANN-1 model, utilizes just the daylight division (nN) as information. The second ANN-2 model has the daylight part and the air temperature (T) as data sources, though the third model (ANN-3) draws in both daylight portion (nN) and noticeable water (w). The fourth ANN-4 model uses as sources of info the (nN) and the extraterrestrial radiation (G0), though the ANN-5 model connects as information three climatic factors, nN, T and the relative mugginess (rh).

In the last ANN-6 model the (w) is added regarding the ANN-5 model. Further, as on account of G, the ANN-1 model predicts QP values utilizing as info the nN just, while the ANN-2 utilizes both nN and T. Conversely, the ANN-3 uses as info variable the G motion rather than T. Further, by including ANN-3 model T as info, the ANN-4 model is shaped, while the ANN-5 model incorporates the (rh) as an extra contribution as for past model. At long last, the ANN-6 model has as contributions up to five parameters, both sunlight based and climatic. For the GUV brilliant motion forecasts, the inferred ANN-1 model evaluations GUV values utilizing as information the air mass (m), while in ANN-2 model the (m) is supplanted by G. The ANN-3 model has as information sources the daylight portion (nN) while the ANN-4 model takes part also the G. The fifth model ANN-5 is framed by adding to the last parameters the extraterrestrial brilliant transition (G0). At long last, the ANN-6 model incorporates as information seven parameters (nN, G, G0, m, T, rh). Review table 2 all the more intently, obviously the daylight (nN) shows up in all ANN models for G forecasts, while for the ANN models evaluating G_{UVB}.

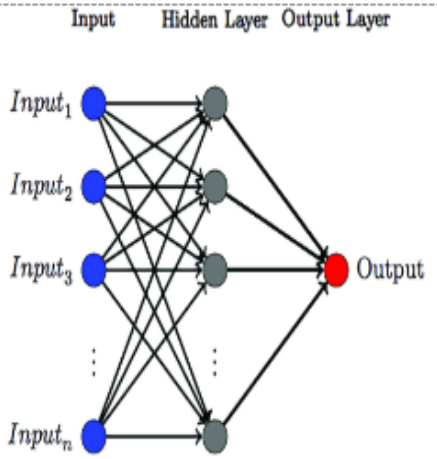

Figure. 2 A schematic representation of a feed forward neural network with one hidden layer.

Table 2 summarizes the ANN-models derived for the broadband solar global G and G_{UV} solar radiant components.

ANN-models for global radiant flux (Gh)	Parameters
ANN-1	nN
ANN-2	nN, T
ANN-3	nN, w
ANN-4	nN, G_o
ANN-5	nN, T, rh
ANN-6	nN, w, T, rh
ANN-models for global PAR radiant flux (QP)	**Parameters**
ANN-1	nN
ANN-2	nN, T
ANN-3	nN, G_h
ANN-4	nN, G_h, T
ANN-5	nN, G_h, T, rh
ANN-6	nN, G_h, G_o, T, rh
ANN-models for global UV radiant flux (GUV)	**Parameters**
ANN-1	m, O_3
ANN-2	G_o, O_3
ANN-3	nN, O_3
ANN-4	nN, G_h, O_3
ANN-5	nN, G_h, G_o, O_3
ANN-6	nN, G_h, G_o, O_3, m, T, rh

5. Results and Discussion

ANN-model results for G solar radiant flux represented by Fig.3 displays predicted global radiant flux values through ANN-1 (Fig. 3a) and ANN-5 (Fig. 3b) models versus measured values. These figures clearly indicate that the simplest ANN-1 and the slightly complicated ANN-5 models provided the lower MBE (%), whereas ANN-2, ANN-3, ANN-4 and ANN-6 models follow in that order. On the other hand, from the RMSE (%) point of view, ANN-2, ANN-1 and ANN-5 models performed better, while ANN-3, 4, and 6 models follow in that order. In general, the MAPE (%) values are always lower than that of RMSE (%). ANN-1 and ANN-5 models provide the lower MAPE values, about 5.9%, while ANN-2, 3, 6 and 4 follow. These findings further verify Will mott and Matsuura's hypothesis [36]. Moreover, results obtained through the ANN-6 models developed here are statistically significant at the particular confidence level of 97.5%, since their t-test values are less than the critical one (tcr it = 1.96). Furthermore, results of the ANN-model statistics are in line with those reported by several researchers in the literature. For example, Behrang et al. (2010) [19], using combinations of meteorological parameters as inputs in ANN-models, reported MAPE (%) values ranging between 5.2 and 9.2%.

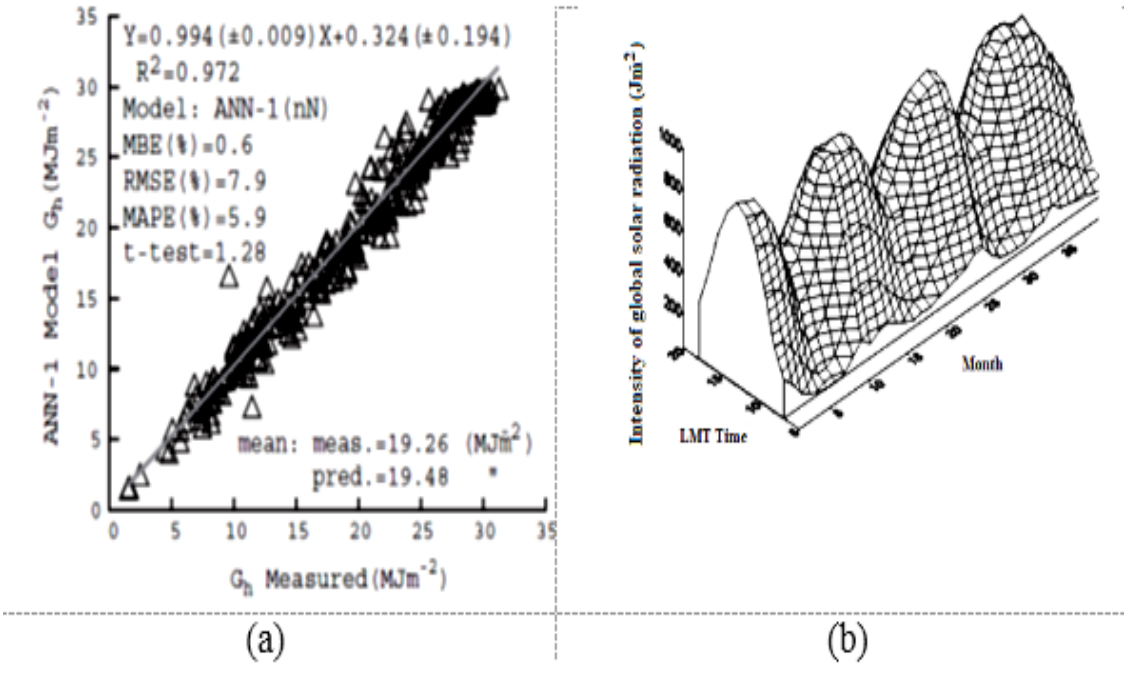

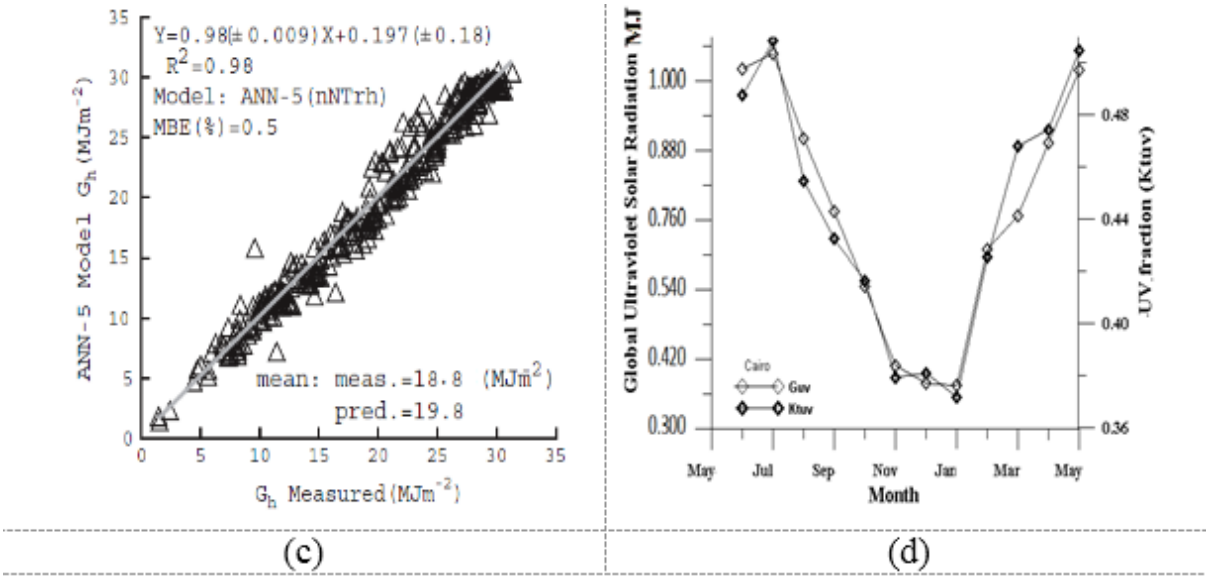

Figure. 3 (a), ANN-1 (c), ANN-5 models, results versus measured data for G solar radiation along with all ANN-models as well as conventional regression models (b) (1MJ=277.78 Wh), and (d) global UV solar radiation (MJ).

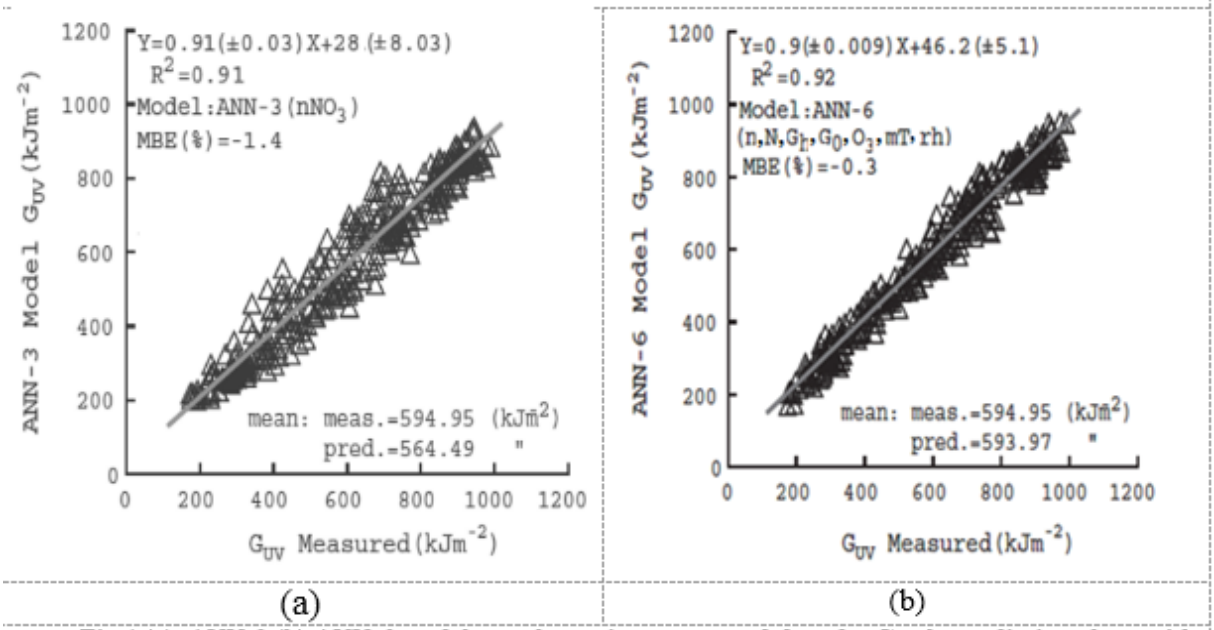

Fig.4 (a), ANN-3 (b) ANN-6 models results various measured data for G solar radiation along with all ANN models as well as Barbero et al. (2006), conventional regression models (b).

Also, Rehman and Mohandes (2008) [20], using air temperature and relative humidity as inputs found MAPE (%) values in the range of 4.5–10.3%, whereas Azadeh et al. (2009) [21] reported an average MAPE (%) value of 6.7% or their ANN-model predictions. Interestingly, the RMSE (%) and MBE (%) values obtained through ANN-models seem to be in line with those reported in the literature by other researchers for the PAR radiant flux. Specifically, Kalogirou, S.K., 2000 [22], and Karoro, A., Ssenyonga, T., Mubiru, J., 2011 [23], for the Spanish environment reported on hourly RMSE (%) values ranging between 8.0% and 21.7% with relevant ANN-models. These values are in good agreement with the present findings of the proposed ANN models. In contrast, the hourly MBE (%) values reported by the aforementioned authors varied between −0.8 and 0.8%, which roughly agree with the present findings through ANN-1, 3 and 5 models. Fig. 3, 4 shows the monthly variation of monthly variation of global and ultraviolet solar radiation .The highest value is in June, while the lowest value is in November. A1 has the highest value in June (237 Wh/m^2/day), while its lowest value is in November (171 Wh/m^2/day). Solar radiant flux Further, Fig. 4 displays selected examples

of scatter plots between ANN-3 (Fig. 4a) and ANN-6 (Fig. 4b) models versus measured UVB radiant flux. As it is mentioned earlier, the UVB radiant flux is affected by cloudiness, optical air mass and ozone column amount, whereas numerous studies reported on the effective correlation between global G_{UVB} radiant flux and G_h (Foyo-Moreno et al., 2003; Alados et al., 2004; Ogunjobi and Kim, 2004; Jacovides et al., 2009) [24-33]. Next, comparisons between the two ANN-models reveal that effective predictors affecting the ultraviolet solar portion may be included in modeling UVB studies.

It is clear that all statistical indicators MBE (%), RMSE (%), MAPE (%) and t-test have been substantially improved when predictors, namely nN, G, G_0, m, T and rh are used as inputs in the ANN-6 model, further verifying earlier suggestions reported by various workers (i.e. Barbero et al., 2006; Junk et al., 2007)[34-36]. It also is underlined here that RMSE (%) and MBE (%) values obtained through all ANN-models are consistent with those reported by other researchers for the UVB radiant flux. Specifically, reported RMSE (%) values ranging between 14.6% and 19.6% with relevant ANN-models applied to the Spanish environment. The present RMSE (%) findings, however, are slightly lower than those of Alados et al.'s. In contrast, MBE (%) values reported for Spain ranging between −0.1 and 1.6%, are of the same order of magnitude with the six candidate ANN-model predictions. Nevertheless, Barbero et al.'s (2006) [35] MBE (%) and RMSE (%) values are much lower than those found here; however, the present ANN-5 and 6 models' MBE (%) results seem to be the exception since they are almost identical to Barbero et al.'s (2006) findings. Interestingly, MBE (%) values reported by Alados et al. (2007) through using only atmospheric parameters as inputs, for Valencia, Santander and La Coruna sites in Spain tend to be consistent with predicted values by the present ANN-5 and 6 models. By contrast, RMSE (%) values reported for all Spanish sites included in Alados et al.'s (2007) analysis are slightly higher than that provided by the ANN-6 models proposed in the present study.

Further, viewing all ANN-models' performances, it is clear that for the simplest ANN-model that used as inputs sunshine variables, n and N, results for RMSE and MBE reveal that for both G, such a combination is sufficient in producing acceptable predictions for the radiant fluxes in question. By contrast, this combination is not sufficient for the G_{UVB} radiant flux. On the other hand, the important role of numerous parameters, both solar and atmospheric mentioned above, for ANN's predictions is further demonstrated through ANN-4 vs. ANN-6 comparison (Fig. 3c). That is, the ANN-4model with nN, G and O_3 as inputs, predicts results with RMSE (%) and MBE (%) of about 9.3% and −0.7% respectively. Whereas in the ANN-6 model by adding G_0, m, T and rh the model's prediction are improved, with RMSE (%) ~ 8.3% and MBE (%) ~ −0.3%. Moreover, it is clear that ANN-6 model's statistical performance is the best since numerous effective parameters, both solar and atmospheric, are included, further verifying results of earlier studies.

The statistical performances of the empirical models are included in Figs. 3c, 4a and 4b for G and G_{UVB} respectively. Furthermore, both Figs. 4a and 3c reveal that the statistical performance of the empirical scheme employed for G results in lower statistical skills than those obtained through the ANN models. It is clear that the statistics of the model tend to approach the ANN-4 model's ones, however, which employs the same variables (nN and G_0), as the conventional model. On the other hand, Figs. 3a produced worse statistics compared to all ANN-model statistics engaged in this analysis.

The Barbero et al.'s (2006) empirical model, clearly overestimates the daily UVB radiant flux values; however, its statistical performance tends to approach statistical results obtained through ANN-1 and 2models proposed in this study for the G_{UVB} radiant flux. It also is clear that results of the conventional model provided RMSE (%) and MAPE (%) values slightly lower than that of the ANN-1 model and slightly higher than the proposed ANN-2 model. Interestingly, predictions of the daily G_{UVB} values through Barbero et al.'s empirical model are statistically significant since its t-test value is less than the critical one. Viewing further the overall results presented here, in principle, as reported by numerous researchers worldwide, most of the parameters likely affecting solar radiant fluxes (water vapor, trace gasses, atmospheric aerosols, clouds' type, extent and distribution in the atmosphere, site's characteristics, ground albedo, geometrical factors, etc.) may result in dissimilar variability UVB solar radiant flux modeling tools. Nevertheless, these parameters could have simultaneous changes which may add up resulting in spectral flux changes up to 30% or even more. On the other hand, several other parameters may inversely impact on the spectral radiant flux changes so that the net result may have an opposite sign compared to the above one, further reflecting the

models' predictions. Therefore, for modeling accuracy of the spectral radiant fluxes it is essential to have as many measurements as possible of these radiant fluxes under diverse environmental conditions.

6. CONCLUSION

Design and analysis of artificial neural network models based on multilayer perceptron for the estimation of daily solar radiant components reveal the feasibility of this tool for predicting G, and G_{UVB} solar radiant fluxes. In this case study, only one hidden layer is sufficient for estimating daily global spectral radiant fluxes through both solar and atmospheric parameters. Sunshine duration plays an important role in obtaining acceptable model predictions, whereas other parameters used may produce conflicting influences on the ANN models' performance. Comparing statistical results for all ANN-models presented in this analysis, it can be concluded that the models ANN-5 (nNTrh) for G_h, ANN-3 (nNGh) for ANN-6 (nN, G, G_0, mT, rh) for G_{UVB} provided the best results. Results obtained through empirically derived schemes, although statistically significant, gave statistical performances that are lower compared to that provided by the ANN-models engaged in this study. Finally, the results obtained in this study render the ANN methodology as a promising alternative to the conventional regression modeling for both broadband and spectral solar radiant flux predictions.

Generally, ANN-6 model by adding G_0, m, T and rh is considered the best model's prediction are improved, with RMSE (%) ~ 8.3% and MBE (%) ~ −0.3%. Moreover, it is clear that ANN-6 model's statistical performance is the best since numerous effective parameters, both solar and atmospheric, are included, further verifying results of earlier studies.

Neural Network Model has been developed for predicting the amount of solar radiation incident on horizontal plates in different bands at different conditions. Because of the variety and complexity of sky radiation, a common assumption made is that the diffuse component of solar radiation (skylight) has an isotropic distribution over the hemispherical sky. On the basis of the results obtained from of this study, we came to this conclusion that Neural Network Model provides an efficient approach for prediction of solar radiations for different spectral bands at different conditions e.g. time, temperature, humidity, etc.

Nomenclature

Clearness index	K_T	Extraterrestrial Radiant flux	G_0
Sunshine fraction.	S/S_0	Standard Division	SD
Global daily ultraviolet	G_{UVB}	Correlation Coefficient	CC
Root mean square error	RMSE	perceptible water	w
Mean Bias Error	MBE	air mass	m
Global solar radiation	G		
Air temperature	T		
Relative Humidity	rh		
Sunshine duration measured	S		
Integrated Sensor Suite	ISS		

REFERENCES

[1] Agar, N. S., Halliday, G. M., Barnetson, R. C., Ananthaswamy, H. N., Wheeler, M., and Jones A. M.: The basal layer in human squamous tumors harbours more UVA than UVB fingerprint mutations: A role for UVA in human skin carcinogenesis, Proceedings of the National Academy of Sciences, 2004, USA, 101,4954–4959.

[2] Al-Aruri, S., Rasas, M., Al-Jamal, K., and Shaban, N.: An assessment of global UV solar radiation in the range (0.290–0.385μm) in Kuwait, 1988, Solar Energy, 41, 159–162.

[3] Ambach,W., Blumthaler, M., and Wendler, G.: A comparison of ultraviolet radiation measured at an arctic and an alpine site, 1991, Solar Energy, 47, 121–126.

[4] W.A. Rahoma, U. Ali Rahoma and A.H. Hassan, Application of Neuro-Fuzzy Techniques for Solar Radiation, 2011, Journal of Computer Science 7 (10): 1605-1611.

[5] Bachelor, M. A. and Bowden, G. T.: UVA-mediated activation of signalling pathways involved in skin tumour promotion and progression, 2004, Seminars in Cancer Biology, 14, 131–138.

[6] Baker-Blocker, A., DeLuisi, J. J., and Dutton, E.: Received ultraviolet radiation in the South Pole, 1984 Solar Energy, 32, 659–662.

[7] Batlles, F. J., Olmo, F. J., and Alados-Arboledas, L.: On the shadow band correction methods for diffuse irradiance measurements, 1995 Solar Energy, 54, 105–114.

[8] Bosch, J. L., L´opez, G., and Batlles, F. J.: Correlating daily solar global irradiation values over complex terrain using artificial neural networks, Proceedings of the "International Forum of Experts in Solar Radiation, SOLARIS 2005, 2nd Joint Conference", Athens, Greek, May 26–27, 2005.

[9] Galli, C., Nardino, M., Levizzani, V., Rizzi, R., and Georgiadis,T.: Radiative energy partition and cloud radiative forcing at a Po valley site, 2004 Atmos. Res., 72, 329–351.

[10] Collares-Pereira, M. and Rabl, A. (1979). The Average Distribution of Solar Radiation-Correlations between Diffuse and Hemispherical and between Daily and Hourly Insolation values., Solar Energy, 22, 155-164.

[11] K. K. Gopinathan &Alfonso Soler, the determination of monthly mean hourly diffuse radiation on horizontal surfaces using equations based on hourly clearness index, sunshine fraction and solar elevation, international journal of solar energy ,volume 18, 1996 - issue 2.

[12] Sokol Dervishi and Ardeshir Mahdavi, Computing diffuse fraction of global horizontal solar radiation: A model comparison, Sol Energy, 2012 Jun; 86(6): 1796–1802.

[13] Marcelo de Carvalho Alves, Luciana Sanches, and José de Souza Nogueira, Effects of Sky Conditions Measured by the Clearness Index on the Estimation of Solar Radiation Using a Digital Elevation Model, Atmospheric and Climate Sciences 03(04):618-626 · January 2013

[14] Gueymard, C.: The sun's total and spectral irradiance for solar energy applications and solar radiation models, 2004, Solar Energy, 76, 423–453.

[15] Fioletov, V. E., Kerr, J. B., McArthur, L. J. B., Wardle, D. I. and Mathews, T.W.: Estimating UV index climatology over Canada, 2003, J. App. Meteorol., 42, 417–433.

[16] Foyo-Moreno, I., Vida, J., and Alados-Arboledas, L.: A simple all-weather model to estimate ultraviolet solar radiation (290– 385 nm), 1999, J. Appl. Meteorol., 38, 1020–1026.

[17] Foyo-Moreno, I., Alados, I., Olmo, F. J., and Alados-Arboledas, L.: The influence of cloudiness on UV global irradiance (295– 385 nm), 2003, Agr. Forest Meteorol., 120, 101–111.

[18] Mosalam Shaltout, A. A. Trabea, Correlation of global solar radiation with meteorological parameters over Egypt, 2000, Renewable Energy 21(2):297-308 ·

[19] Behrang, M.A., Assareh, E., Ghanbarzadeh, A., Noghrehabadi, A.R., 2010. The potential of different artificial neural network (ANN) techniques in daily global solar radiation modelling based on meteorological data. Sol. Energy 84, 1468–1480.

[20] Rehman, S., Mohandes, M., 2008, Artificial neural network estimation of global solar radiation using air temperature and relative humidity, Energy Policy 36, 571–576.

[21] Azadeh, A., Maghsoudi, A., Sohrabkhami, S., 2009, An integrated artificial neural networks approach for predicting global radiation, Energy Convers. Manag. 50 (6), 1497–1505.

[22] Kalogirou, S.K., 2000. Applications of artificial neural networks for energy systems., Appl. Energy 67 (1–2), 17–35.

[23] Karoro, A., Ssenyonga, T., Mubiru, J., 2011. Predicting global solar radiation using an artificial neural network single-parameter model,. Adv. Artif. Neural Syst. http://dx.doi.org/10.1155/2011/751908, (Article ID 751908, 7 pages).

[24] Foyo-Moreno, I., Alados, I., Olmo, F.J., Alados-Arboledas, I., 2003. The influence of cloudiness on UV global irradiance (295–385 nm),. Agric. For. Meteorol. 120, 101–111.

[25] Alados, I., Gomera, M.A., Foyo-Moreno, I., Alados-Arboledas, L., 2007. Neural network for the estimation of UV erythemal irradiance using solar broadband irradiance,. Int. J. Climatol. 27, 1791–1799.

[26] Ogunjobi, K.O., Kim, Y.J., 2004. Ultraviolet (0.280–0.400 μm) and broadband solar hourly radiation atKwangju, South Korea: analysis of their correlation with aerosol optical depth and clearness index. Atmos. Res. 71, 193–214.

[27] Jacovides, C.P., Kontogianis, H., 1995. Statistical procedure for the evaluation of evapotranspiration computing models,. Agric. Water Manag. 27, 365–371.

[28] Jacovides, C.P., Gianourakos, G.P., Asimakopoulos, D.N., Steven, M.D., 1998. M Measured spectra of solar ultraviolet irradiances at Athens basin, Greece,. Theor. Appl. Climatol. 59, 107–119.

[29] Jacovides, C.P., Tymvios, F.S., Papaioannou, G., Asimakopoulos, D.N., Theofilou, C.M., 2004. Ratio of PAR to broadband solar radiation measured in Cyprus. Agric. for Meteorol. 121, 135–140.

[30] Jacovides, C.P., Tymvios, F.S., Assimakopoulos, V.D., Kaltsounides, N.A., 2007. The dependence of global and diffuse PAR radiation components on sky conditions at Athens, Greece. Agric. for Meteorol. 143, 277–287.

[31] Jacovides, C.P., Tymvios, F.S., Asimakopoulos, D.N., Kaltsounides, N.A., Theoharatos, G.A., Tsitouri, M., 2009. Solar global UVB (280–315 nm) and UVA (315–380 nm) radiant fluxes and their relationships with broadband global radiant flux at an eastern Mediterranean site,. Agric. for Meteorol. 149, 1188–1200.

[32] Jacovides, C.P., Boland, J., Rizou, D., Kaltsounides, N.A., Theoharatos, G.A., 2012. School Students participation in monitoring solar radiation components: preliminary results for UVB and UVA solar radiant fluxes Renew. Energy 39, 367, 374. Iqbal, M.: An introduction to solar radiation, Academic Press, 1983.

[33] Iziomon, M. G., Mayerb, H., and Matzarakisb, A.: Downward atmospheric longwave irradiance under clear and cloudy skies: Measurement and parameterization, 2003, J. Atmos. Sol-Terr. Phy., 65, 1107–1116.

[34] Barbero, F.J., Lopez, G., Batlles, F.J., 2006. Determination of daily solar ultraviolet radiation using statistical models and artificial neural networks, Ann. Geophys,. 24, 2105–2114.

[35] Bat-Oyun, T., Shinoda, M., Tsubo Junk, J., Feister, U., Helbig, A., 2007. Reconstruction of daily solar UV irradiation from 1893 to 2002 in Potsdam, Germany,. Int. J. Biometeorol. 5, 505–512.

[36] Sapolsky R. M., Mott G. E. 1987. Social subordinance in wild baboons is associated with suppressed high density lipoprotein-cholesterol concentrations: the possible role of chronic social stress,. Endocrinology. 121: 1605–1610.

APPENDIX

One of the most common indicators used in error analysis is the mean absolute error. This term is used similar to variance. The MAE of an estimator y_j with respect to the estimated parameter x_j is defined as:

$$\mathrm{MAE} = \frac{1}{n}\sum_{j=1}^{n}\left|y_j - x_j\right| \tag{5}$$

where, n is the number of data points. The MAPE is measure of accuracy in a fitted time series.

$$\mathrm{MAPE} = \frac{1}{n}\sum_{j=1}^{n}\left|\frac{y_j - x_j}{y_j}\right| \tag{6}$$

We used the MBE to describe how much the predictor underestimates or overestimates the situation. The MBE was determined using the following equation:

$$\mathrm{MBE} = \frac{\sum_{j=1}^{n}\left(\frac{y_j - x_j}{x_j}\right)}{n} \tag{7}$$

The SD is the standard deviation of the sampling distribution and may be estimated by the formula $\frac{\mathrm{SD}}{\sqrt{n}}$ where SD is the standard deviation of the population distribution. The mean squared error (MSE) of an estimator is the square of the amount by which the estimator differs from the quantity to be estimated. The difference occurs because the estimator doesn't account for information that could produce a more accurate estimate. The RMSE which gives an idea of the magnitude of the non-systematic error is then simply defined as the square root of the MSE. The mathematical formula of the RMSE is given by:

$$\mathrm{RMSE} = \sqrt{\frac{\sum_{J=1}^{n}\left(y_j - x_j\right)^2}{n}} \tag{8}$$

In general, correlation coefficient, CC, indicates the strength and direction of a linear relationship between two random variables. The correlation is 1 in the case of an increasing linear relationship, -1 in the case of a decreasing linear relationship, and some value in between in all other cases, indicating the degree of linear dependence between the variables.

$$CC = \frac{\sum_j \left(y_j - \bar{y} \right) . \left(x_j - \bar{x} \right)}{\left\{ \left[\sum_j \left(y_j - \bar{y} \right)^2 \right] . \left[\sum_j \left(x_j - \bar{x} \right)^2 \right] \right\}^{0.5}} \quad (9)$$

Where, $\bar{x}$ is the observed mean value and $\bar{y}$ is the predicted mean value.

Citation: *Samy A. Khalil, et.al., (2020). Statistical Evaluation of Global and Ultraviolet Solar Radiation by Using Artificial Neural Networks. International Journal of Advanced Research in Physical Science (IJARPS) 7(6), pp. 3-13 2020.*